Reply to Anonymous Referee #1

We thank the reviewer for the careful reading of the manuscript and helpful comments. We have revised the manuscript following the suggestion, as described below.

General comments

This paper uses a cloud-resolving fully coupled WRF-Chem model to investigate the respective roles of aerosol-radiation interactions (ARIs) and aerosol-cloud interactions (ACIs) on a winter snowfall event in the Guanzhong Basin and its surrounding areas. The study systematically separates the contributions of ARIs and ACIs through a combination of anthropogenic emission scaling and ARIs on/off experiments. Overall, I think it is a solid work with a well-designed suite of sensitivity experiments. I suggest publishing it after addressing the following comments with a major revision.

Specific comments

1 Comment: The title and abstract emphasizes snowfall event, but the main text lacks a focused description of this event. It is recommended to either add a more detailed description of the event, or revise the abstract and title to reflect the broader scope.

Response: In the original manuscript, we have primarily described the large-scale synoptic background (cold front, wind fields, moisture transport, etc.). To better align the main text with the title and abstract, we have enriched Section 3.1 by adding a more direct characterization of the snowfall event itself, while retaining the original synoptic description. Specifically, we have added information on the temporal evolution of snowfall intensity, the multi-peak structure of the hourly snowfall rate, and the coexistence of persistent snowfall with high $PM_{2.5}$ concentrations over the GZB. This makes the description more focused on the "snowfall event" as presented in the title and abstract.

The revisions in L178-184 of Section 3.1 are as follows,

"*3.1 Snowfall event overview*

A heavy snowfall event occurred from 26 to 28 January 2022 is investigated in GZB+GZBs, with the total precipitation of 6.4 mm, and the maximum daily precipitation of 2.3 mm is on January 28. The snowfall event is basically the result of the interaction between the northerly cold air and southerly and easterly warm air in low-level atmosphere, as a cold front system proceeds from the North China (January 25) to the south-east (January 26-27) and then south-

west direction (January 28) mainly along the coast (Figure S1). GZB+GZBs is located to the southwest (January 25), the west (January 26) and the northwest (January 27-28) side of the cold front, which is not the main area of the precipitation that occurred near the cold front. During January 26 to 28, there is clear evidence of weak cold air incursion in the GZB+GZBs at 925 hPa (Figures S2a-c). At 850 and 700 hPa (Figures S2d-i), the weak cyclonic wind shear and positive vorticity are maintained in the GZB during the event. At 500 hPa (Figures S2j-l), GZB+GZBs is situated in the front of a very shallow trough, which is favorable for the development of low-level convergence, and eventually leads to the snowfall event in this area. The low-level water vapor is brought to the snowfall area mainly by the southwesterly and easterly airflow from Bay of Bengal and the South China Sea. The snowfall event lasts approximately 72 hours from 00 LT 26 to 00 LT 29 January 2022. The observed hourly snowfall rate (Figure 4) shows a multi-peak structure, with the maximum instantaneous rate reaching ~0.21 mm h^{-1} *around 12 LT 28 January. The majority of the precipitation at the surface is in the form of snow, as the near-surface temperature during the event remains between -4℃ and 0℃ (Figure S2). Despite the continuous snowfall, the observed* $PM_{2.5}$ *concentrations (*$[PM_{2.5}]$*) remain high, with an average of 108.5 and 74.1 μg* m^{-3} *in GZB and GZBs (Figure 2a), respectively, providing a unique polluted environment to investigate aerosol-snowfall interactions.*"

2 Comment: Lines 129-131: The authors stated that F_ARI0 is setup by not considering ARI. Could you add more details about how do you remove ARI in the model?

Response: We have added detailed information on the setting of F_ARI0 cases in Lines 147-149 as follows,

"*The second group of sensitivity simulations is the same as the F_BASE, but the ARI effect is not considered (hereafter referred as to F_ARI0). In the F_ARI0 experiment, the aerosol effect on solar radiation is not considered in the shortwave radiation transfer module in the WRF-Chem model, such that aerosols no longer modify atmospheric heating rates and further influence meteorological fields. The model setup is the same for all experiments, except for the anthropogenic emission amplitude and the option of ARIs (on or off). In the F_BASE, the member with the AESF of 1.0 is referred to as the benchmark simulation (CTRL), which is used to validate the model performance.*"

3 Comment: Section 2.1: The 19 AESF values are not explicitly listed. If possible, please correct this and consider adding the full list of scale factors for clarity.

Response: We have explicitly listed all AESF values used in the sensitivity simulations for clarity. The complete list of scale factors has been provided in the Supplementary Information as follows,

Line 132 in the manuscript: "*A set of 19 anthropogenic emission scale factor (AESF) is used in sensitivity simulations, ranging from* 2^{-3} *to* 2^{3} *with an exponential increasing step of 1/3 (Table S2)*."

Table S2. Planetary boundary layer height (PBLH) averaged over the GZB+GZBs for each anthropogenic emission scale factor (AESF) in the F_BASE from 26 to 28 January 2022.

Index	*AESF Value*	*PBLH (m)*
1	*0.125*	*452.7*
2	*0.157*	*451.1*
3	*0.198*	*449.7*
4	*0.250*	*447.5*
5	*0.315*	*445.0*
6	*0.397*	*441.9*
7	*0.500*	*438.4*
8	*0.630*	*434.3*
9	*0.794*	*428.9*
10	*1.000*	*422.9*
11	*1.260*	*415.4*
12	*1.587*	*406.2*
13	*2.000*	*395.4*
14	*2.520*	*382.7*
15	*3.175*	*369.3*
16	*4.000*	*354.0*
17	*5.040*	*338.2*
18	*6.350*	*320.3*
19	*8.000*	*299.6*

4 Comment: Figure 2: Only a brief comparison between the observations and simulations of $PM_{2.5}$ and SO_2 in Figure 2 was presented, without covering the comparison of O_3 and NO_2. Is there a particular reason why these two variables are emphasized here? Some differences can also be observed from Figures 2b and 2c.

Response: We have added further discussions on the model performance for O_3 and NO_2 in Lines 190-195 of the revised manuscript as follows,

"*The simulated [$PM_{2.5}$] are generally more than 75 μg* m^{-3} *in the GZB, but the* SO_2 *level is not high in GZB and GZBs, less than 20 μg* m^{-3}. *The model tends to underestimate* O_3 *and* *overestimate NO_2 concentrations in the GZB when comparing to observations. During wintertime, near-surface O_3 concentrations are strongly influenced by NO titration effects, and the overestimation of NO_2 concentrations might partly contribute to the underestimation of O_3 concentrations in the simulations. The NO_2 overestimation might be associated with uncertainties in the anthropogenic emission inventory or PBLH simulations.*"

5 Comment: Section 3.2: The simulation assessment section directly states that the simulations all underestimated air pollution, but does not provide the reasons for this. It is suggested to include a brief discussion on the possible causes of the simulation deviation.

Response: We have added a brief discussion on the possible causes of the simulation biases in Lines 206-209 of the revised manuscript as follows,

"*In general, the model slightly underestimates the air pollutants concentrations against observations, with the NMB ranging from -8.4% to -2.3%. These underestimations may partly result from uncertainties in anthropogenic emissions, meteorological fields, and chemical or physical parameterizations in the model, which can influence air pollutant accumulation and secondary formation processes during wintertime (Bei et al., 2017; Cheng et al., 2021; Li et al., 2025).*"

Bei, N., Wu, J., Elser, M., Feng, T., Cao, J., El-Haddad, I., Li, X., Huang, R. J., Li, Z., Long, X., Zhao, S., Tie, X., Prévôt, A. S. H., and Li, G.: Impacts of meteorological uncertainties on the haze formation in Beijing–Tianjin–Hebei (BTH) during wintertime: a case study, Atmos. Chem. Phys., 17, 14579–14591, https://doi.org/10.5194/acp-17-14579-2017, 2017.

Cheng, Y., Yu, Q.-Q., Liu, J.-M., Zhu, S., Zhang, M., Zhang, H., Zheng, B., and He, K.-B.: Model vs. observation discrepancy in aerosol characteristics during a half-year long campaign in Northeast China: the role of biomass burning, Environ. Pollut., 269, 116167, https://doi.org/10.1016/j.envpol.2020.116167, 2021.

Li, Z., He, Y., Yu, S., Wang, H., Fan, F., Qin, C., Chen, Y., Dai, W., Jin, Z., and Zhao, D.: Intercomparison of multiple chemical mechanisms in simulating severe haze event over the North China Plain, Atmos. Environ., 361, 121439, https://doi.org/10.1016/j.atmosenv.2025.121439, 2025.

6 Comment: Figure 4: It was pointed out that in Figure 4, five peaks were successfully simulated, but two of the peaks were significantly lower. Are there any studies that can explain the reasons for the low values of these two simulations? It was also found that there was a low-value simulation result that was much higher than the observation. Could this also be presented?

Response: We have added discussions in Section 3.2 to clarify the model bias in the simulated precipitation shown in Figure 4.

In lines 216-222: "*These underestimations are likely related to the model's sensitivity to initial conditions and its performance during the spin-up and decay stages of the event, respectively, especially given that the precipitation occurs on the periphery of the cold front where large-scale forcing is weak (Liu et al., 2018; Lin et al., 2023). Additionally, the model also produces higher light precipitation during 27-28 January compared to the observations. As shown by Liu et al. (2024), the lack of a shallow convection scheme at gray-zone resolutions (i.e., 6 km) allows excessive low-level moisture to accumulate and prematurely convert to light precipitation under stratiform conditions. These localized discrepancies do not compromise the model's overall performance.*"

Lin, Q., Chen, J., Ou, T., Lai, H.-W., Prein, A. F., and Chen, D.: Performance of the WRF model at the convection-permitting scale in simulating snowfall and lake-effect snow over the Tibetan Plateau, J. Geophys. Res.-Atmos., 128, e2022JD038433, https://doi.org/10.1029/2022JD038433, 2023.

Liu, J., Yang, K., Wang, J., Zhou, X., Jiang, Y., Shao, C., Lu, H., Yao, X., Sun, J., and Shi, J.: Impacts of a shallow convection scheme on kilometer-scale atmospheric simulations over the Tibetan Plateau, Clim. Dyn., 62, 8019–8034, https://doi.org/10.1007/s00382-024-07330-0, 2024.

Liu, L., Ma, Y., Menenti, M., Zhang, X., and Ma, W.: Evaluation of WRF modeling in relation to different land surface schemes and initial and boundary conditions: A snow event simulation over the Tibetan Plateau, J. Geophys. Res.-Atmos., 124, 209–226, https://doi.org/10.1029/2018JD029208, 2019.

7 Comment: Lines 184 and 203: Where can we see the extent of the decline that "the PBLH is decreased by about 34% in GZB+GZBs"? It was later found that "PBLH over GZB+GZBs decreases from about 450 m to 300 m" in line 203. Are these two statements related to each other? If so, it would be better to present the specific values alongside the percentage at the first mention to improve clarity. Moreover, the specific values (450 m and 300 m) are presented without a clear reference to a figure or table. It is recommended to either add a figure showing the PBLH variation with AESF, or explicitly indicate that this result is derived from model output statistics

Response: We agree that the relationship between the percentage decrease (34%) and the absolute values (450 m to 300 m) should be made explicit at the first mention, and that a reference is needed. We have made the following clarification:

In lines 239-240: "*Sensitivity results show that when the AESF increases from 0.125 to 8.0, the PBLH in GZB+GZBs decreases from approximately 450 m to 300 m, a reduction of about 34% based on model output statistics (see Table S2 for detailed values).*"

Table S2. Planetary boundary layer height (PBLH) averaged over the GZB+GZBs for each anthropogenic emission scale factor (AESF) in the F_BASE from 26 to 28 January 2022.

Index	AESF Value	PBLH (m)
1	0.125	452.7
2	0.157	451.1
3	0.198	449.7
4	0.250	447.5
5	0.315	445.0
6	0.397	441.9
7	0.500	438.4
8	0.630	434.3
9	0.794	428.9
10	1.000	422.9
11	1.260	415.4
12	1.587	406.2
13	2.000	395.4
14	2.520	382.7
15	3.175	369.3
16	4.000	354.0
17	5.040	338.2
18	6.350	320.3
19	8.000	299.6

8 Comment: Figure 7: The figure presents only the difference in vertical velocity between F_BASE and F_ARI0. The convergence phenomenon mentioned in the text cannot be directly derived from this graph. Additional diagnostics are needed to support this claim.

Response: We agree that the statement "enhanced convergence by the ARI-induced downward motion" cannot be directly inferred from the vertical velocity difference shown in Figure 7b alone, as convergence is fundamentally a property of the horizontal wind field. To address this issue, we have performed an additional diagnostic analysis and present the results in the newly added Figure SX (Supplement).

In lines 297-302: "*These ARI-induced variations in divergence and water vapor flux are shown in Figure S5. ARIs induce divergence (positive values) below approximately 700 m and convergence (negative values) above this level, with the convergence strengthening as AESF increases. Correspondingly, negative water vapor flux anomalies occur within the divergent layer, indicating moisture export from the lower troposphere, while positive anomalies occur within the convergent layer aloft, indicating moisture accumulation. This circulation pattern contributes to the drying of the PBL.*"

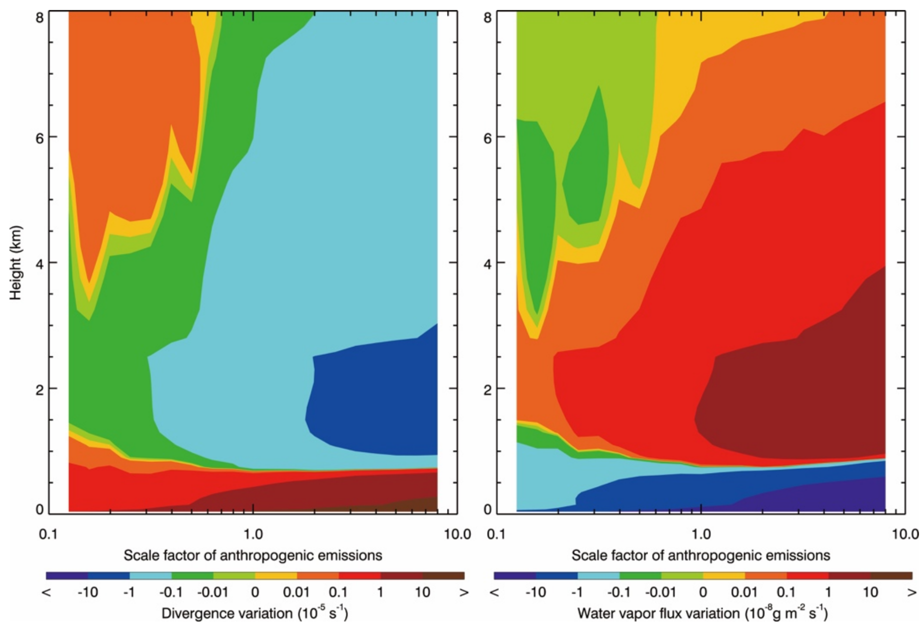

Figure S5: *Profile variation of horizontal (a) divergence and (b) water vapor flux averaged over GZB+GZBs from 26 to 28 January 2022 caused by ARIs, as a function of the scale factor of anthropogenic emissions. For the divergence variations, negative values indicate that ARIs enhance convergence, whereas positive values indicate enhanced divergence. For the water vapor flux variations, positive values indicate enhanced moisture inflow into the region, while negative values indicate enhanced moisture outflow from the study region.*

9 Comment: Line 236: The statement that "decreasing RHW also explain the slow increase of the CND" is problematic because it uses one outcome of ACIs to explain another. A more straightforward explanation—such as how lower RHW makes it harder for CCN to activate, limiting the increase in CND—would be more logical and easier to follow.

Response: We have revised the sentence to provide a more direct and physically based explanation in lines 332-335 as follows, "*Therefore, decreasing RHI with increasing AESF causes the decreasing trend of the CND with the AESF. In addition, the ACI-induced decrease in RHW provides a physical explanation for the relatively slow increase of cloud droplet CND with AESF (Figure 8a), as lower RHW makes it more difficult for the additional CCN (from increased emissions) to activate into cloud droplets, thus limiting the rate of CND increase.*"

10 Comment: Line 268: As can be seen from Figure 8a, CND does not decrease as Reffc does with the increase of AESF. Only when WIth ARI and it is greater than a certain value will it be reduced.

Response: We have revised the relevant sentences in Section 3.4 to provide a more accurate description of the relationships among R_{effc}, CND, and CWP. The revised text in lines 375-380 as follows,

"*Figure 10a shows the variation of p-mean of cloud droplet effective radius (R_{effc}) with the AESF in F_BASE and F_ARI0. R_{effc} decreases with increasing AESF in the F_BASE and F_ARI0, which is well consistent with the variation of CND and CWP of cloud droplets. R_{effc} decreases with increasing AESF in both experiments. This decrease is primarily driven by the simultaneous decrease in CWP (Figures 9a and 9b). In the F_ARI0, although CND increases monotonically with AESF (Figure 8a), the reduction in CWP dominates, leading to a decreasing R_{effc}. In the F_BASE experiment, R_{effc} continues to decrease even when CND begins to decline after AESF exceeds 2.5 (Figure 8a), reflecting the dominant role of CWP reduction.*"

11 Comment: Section 3.5: Why was it specifically pointed out that Figure 11a does not take into account the ARI situation? This increase is too small, and it is even smaller compared to the increase trend when ARI is considered.

Response: We thank the reviewer for this insightful suggestion. We agree that the increasing trend of precipitation with AESF in the F_ARI0 experiment is very small. We would like to clarify why we specifically pointed out this small increase. Our intention is to highlight a contrast with previous studies over the same region. Yang et al. (2013a, b) and Bei et al. (2025) have reported that ACIs suppress precipitation in the GZB. In contrast, our F_ARI0 results show a weak but non-negative response of total precipitation to increasing aerosols under this particular snowfall event. We believe this contrast is meaningful because it suggests that the net effect of ACIs on wintertime snowfall may differ from their effect on warm-season convective rainfall. The small magnitude of the increase also indicates that the invigorating effect of ACIs on ice-phase precipitation only marginally outweighs the suppressing effect on warm rain, resulting in a near-neutral net effect.

We have therefore revised the relevant paragraph in Section 3.5 to more accurately reflect the subtlety of these findings as follows,

In lines 390-392 and lines 402-404: "*Considering the difference in aerosol concentrations between GZB and GZBs, we discuss the impact of aerosols on precipitation in each region separately. Figure 11a provides the variation of the average 3-day accumulative precipitation in the GZB with the AESF. When ARIs are excluded (F_ARI0), the accumulative precipitation exhibits a weak increasing trend with the AESF, which is not consistent with previous studies over the GZB that have reported a suppression effect of ACIs on precipitation (e.g., Yang et al., 2013a, b; Bei et al., 2015). Yang et al. (2013a, b) have correlated the decreasing trend of precipitation inside the GZB with deterioration of the air pollution, revealing the microphysically suppressive effect of increased aerosols on precipitation. Bei et al. (2025) have also shown that ACIs tend to decrease convective precipitation in the GZB based on sensitivity simulations of a summertime short-term heavy rainfall event. In this study, as we have discussed above, increasing anthropogenic emissions decrease CWP and Reffc, lowering the conversion of cloud water to rainwater to decrease the liquid-phase precipitation. However, increasing emissions increase IWP and Reffi, facilitating the formation and growth of snow flakes to enhance the ice-phase precipitation. Figure 12 shows dependence of the liquid-phase and ice-phase precipitation at the ground surface in the GZB with the AESF. Overall, liquid-phase precipitation is lower at higher AESF, while ice-phase precipitation is higher. The increase in ice-phase precipitation partly compensates for the decrease in liquid-phase precipitation, leading to a net weak increase in total precipitation over the GZB for higher AESF (Figure 11a).*"

12 Comment: Figure 11: It shows that the precipitation of GZB and GZBs has opposite responses to the increase in emissions. However, the article does not provide a comparison of the meteorological fields and cloud microphysics background of the two regions, which makes the explanation for "why they are opposite" somewhat weak. It is suggested to add an additional figure to illustrate the differences between GZB and GZBs in terms of the RH contour, the vertical distribution of cloud water/ice water, and the proportion of liquid water paths.

Response: We have included additional figures to show the differences between GZB and GZBs in terms of the vertical distribution of RH, cloud water content and ice water content (Figure SX2), as well as the proportion of liquid water paths (Figure SX3) as a function of the scale factor of anthropogenic emissions. We have also added discussions in Lines 432-440 as follows,

"*In the GZBs, without ARIs, ACIs decrease precipitation with increasing AESF (Figure 11c), and ARIs also appreciably decrease the precipitation with the same AESF (Figures 11c and 11d), which are generally contrary to those in the GZB (Figures 11a and 11b). There are two reasons that can explain the different responses of precipitation to ARIs and ACIs in the GZB and GZBs. In the F_ARI0 without ARIs, the variation of liquid-phase and ice-phase precipitation with increasing AESF in the GZBs is similar to those in the GZB. However, the ratio of liquid-phase precipitation to the total precipitation varies considerably in the GZB and GZBs. The proportion of liquid water path is consistently higher in GZBs than GZB across all emission scenarios (Figure S9). For example, in the REF0, the ratio in the GZB is 2.5%, but in the GZBs, it is 9.1%. To further understand the contrasting precipitation responses between GZB and GZBs, the background thermodynamic and cloud microphysical conditions of the two regions are compared in the F_BASE (Figure S10). Compared with GZB, GZBs exhibit higher lower-tropospheric relative humidity, substantially larger cloud water content, and smaller ice water content above 6 km. Therefore, aerosol-induced perturbations to liquid cloud microphysics are expected to exert a stronger influence on precipitation in GZBs, providing a physical basis for the contrasting precipitation responses shown in Figure 11.*"

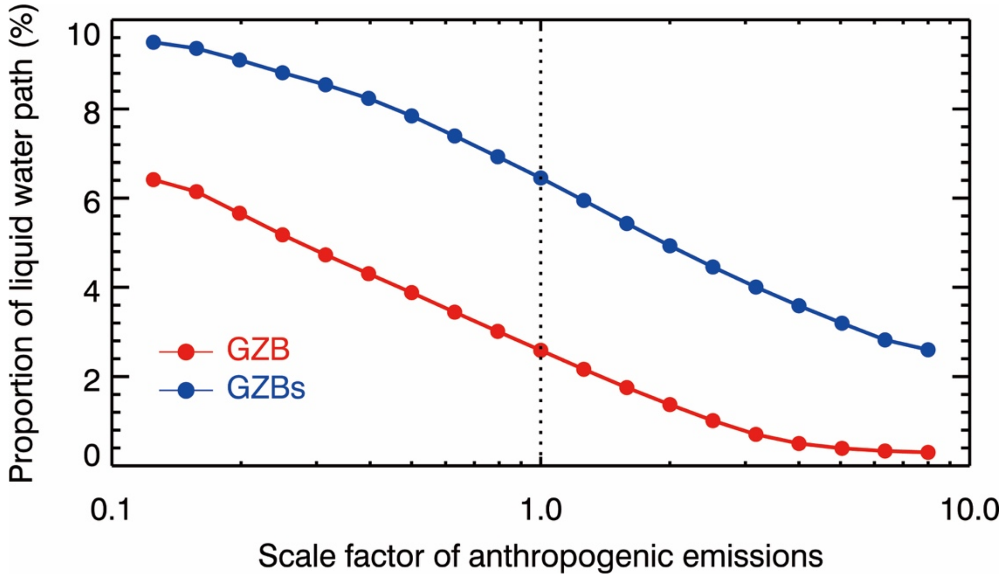

Figure S9: The proportion of liquid water paths over GZB and GZBs from 26 to 28 January

2022 in the F_BASE, as a function of the scale factor of anthropogenic emissions.

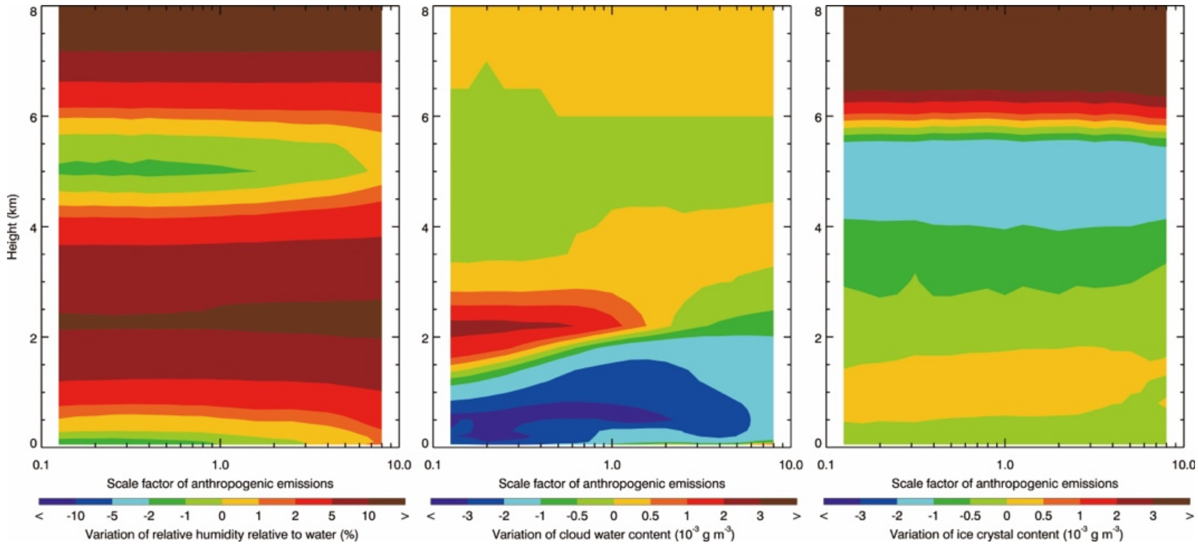

Figure S10: Profile differences between GZB and GZBs of average (a) relative humidity, (b) cloud water content, and (c) ice water content over GZB+GZBs from 26 to 28 January 2022, as a function of the scale factor of anthropogenic emissions.

13 Comment: Line 260: It would be better to add "As can be seen from Figure 9c, " at the beginning of this sentence to explicitly link the statement to the corresponding figure.

Response: We have revised the sentence in line 359 as "*Therefore, as can be seen from Figure 9c, although ACIs decrease RHI with increasing AESF, the ice water path (IWP) shows an increasing trend with the AESF.*"

Reply to Anonymous Referee #2

This manuscript investigates the impacts of anthropogenic aerosols on a winter snowfall event over the Guanzhong Basin using WRF-Chem, with a focus on disentangling aerosol–radiation interactions (ARIs) and aerosol–cloud interactions (ACIs). The topic is scientifically important, especially given the large uncertainties in aerosol–precipitation interactions under polluted conditions. The study is generally well structured, and the model reasonably reproduces observed pollutants and precipitation. The attempt to separate ARI and ACI contributions and the identification of contrasting responses between GZB and surrounding regions are valuable. However, the manuscript still has several critical issues in physical interpretation, experimental design, and result robustness, which need to be addressed before publication.

1 Comment: Wet scavenging refers to the effect of precipitation on aerosols, rather than the influence of aerosols on precipitation. In addition, the phrase "decreased solar radiation" is not appropriate to describe the impact of aerosols on precipitation.

Response: We have removed "wet scavenging" from the sentence and have revised "decreased solar radiation" to a more accurate description in lines 42-44 as follows,

"*Past studies have proposed many mechanisms about aerosol effects on precipitation, such as the positive precipitation-aerosol relationships attributed to invigoration effect (e.g., Khain et al., 2005; Pinsky et al., 2013; Rosenfeld et al., 2008), the negative aerosol effect on precipitation due to cloud water competition (e.g., Albrecht, 1989; Rosenfeld, 1999), and ARIs that reduce solar radiation down to the surface and modify atmospheric temperature profiles (e.g., Ackerman et al., 2000; Koren et al., 2004).*"

2 Comment: As shown in Figure 3, compared with the simulation results of $PM_{2.5}$, O_3, and NO_2, the simulation errors of SO_2 are relatively larger. The authors should provide a clear explanation for these discrepancies.

Response: We have added a concise explanation specifically for SO_2 in lines 198-205 of the revised manuscript as follows,

"*However, the model does not show good performance in simulating the SO_2 temporal variation, with an IOA of 0.25. The larger discrepancy for SO_2 mainly results from the sensitivity of point-source SO_2 simulations to meteorological uncertainties. The transport and dispersion of SO_2 from point sources (i.e., power plants and industrial facilities) are highly* *sensitive to the accuracy of simulated wind fields (Hu et al., 2022). In the GZB, complex terrain and weak synoptic forcing further increase the uncertainty in meteorological simulations (Bei et al., 2017b). Additionally, parameterizations of SO_2 oxidation, including aqueous-phase and heterogeneous pathways, under the persistent high-RH conditions during this snowfall event also introduces further uncertainties (Travis et al., 2025).*"

Bei, N., Zhao, L., Xiao, B., Meng, N., and Feng, T.: Impacts of local circulations on the wintertime air pollution in the Guanzhong Basin, China, Sci. Total Environ., 592, 373–390, https://doi.org/10.1016/j.scitotenv.2017.02.151, 2017b.

Hu, Y., Zang, Z., Chen, D., Ma, X., Liang, Y., You, W., Pan, X., Wang, L., Wang, D., and Zhang, Z.: Optimization and evaluation of SO2 emissions based on WRF-Chem and 3DVAR data assimilation, Remote Sens., 14, 220, https://doi.org/10.3390/rs14010220, 2022.

Travis, K. R., Nault, B. A., Crawford, J. H., Kim, H., Chen, Q., Zheng, Y., Liu, T., Jimenez, J. L., Campuzano-Jost, P., Wennberg, P. O., Crounse, J. D., and Huey, L. G.: Year-round analysis of multiphase sulfate production in aerosol particles in East Asia, ACS ES&T Air, 2, 1758–1769, https://doi.org/10.1021/acsestair.5c00136, 2025.

3 Comment: The boundary between the Guanzhong Basin (GZB) and its surrounding areas (GZBs) should be added in all figures to improve readability. Furthermore, the comparison of accumulated precipitation results should be separated between GZB and GZBs to ensure that no systematic differences are overlooked.

Response: We have modified Figures 1, 2, 5, and 14 as suggested. We have also modified Figures 4 and 5 to increase the rain rate comparison over GZB and GZBs. We have added discussions in Lines 211-216 as follows,

"*Figure 4 provides the temporal variation of precipitation rates averaged at meteorological sites in GZB+GZBs from 26 to 28 January. The model generally reproduces the temporal evolution of the observed hourly precipitation, with NMBs of -3.3%, -7.4%, and -1.3% and IOAs of 0.85, 0.75, and 0.78 over GZB+GZBs, GZB, and GZBs, respectively. The observed five rainrate peaks are successfully reproduced in all regions, but the underestimation of the first and fifth rainrate peak is considerable in GZB+GZBs. Compared with GZB, the model exhibits better overall performance in GZBs, while a larger underestimation is found over GZB during periods of intense precipitation. These underestimations are likely related to the model's sensitivity to initial conditions and its performance during the spin up and decay stages of the event, respectively, especially given that the precipitation occurs on the periphery of the cold front where large scale forcing is weak (Liu et al., 2018; Lin et al., 2023). Additionally, the* *model also produces higher light precipitation during 27-28 January compared to the observations. As shown by Liu et al. (2024), the lack of a shallow convection scheme at gray zone resolutions (i.e., 6 km) allows excessive low level moisture to accumulate and prematurely convert to light precipitation under stratiform conditions. These localized discrepancies do not compromise the model's overall performance. The pattern comparison of the 3-day accumulative precipitation over the GZB and GZBs is shown in Figure 5. The model generally replicates the precipitation distribution compared to the observations (Figure 5a). For all stations in GZB+GZBs, the simulated accumulated precipitation agrees reasonably well with observations, with an NMB of -3.7% and an IOA of 0.85 (Figure 5b). When evaluated separately, the model yields NMBs of -10.2% and -1.3% over GZB and GZBs, respectively, indicating that the underestimation is mainly concentrated within the basin region. Nevertheless, the relatively high IOAs of 0.89 and 0.85 over GZB and GZBs suggest that the model adequately captures the spatial variability of precipitation in both regions.*"

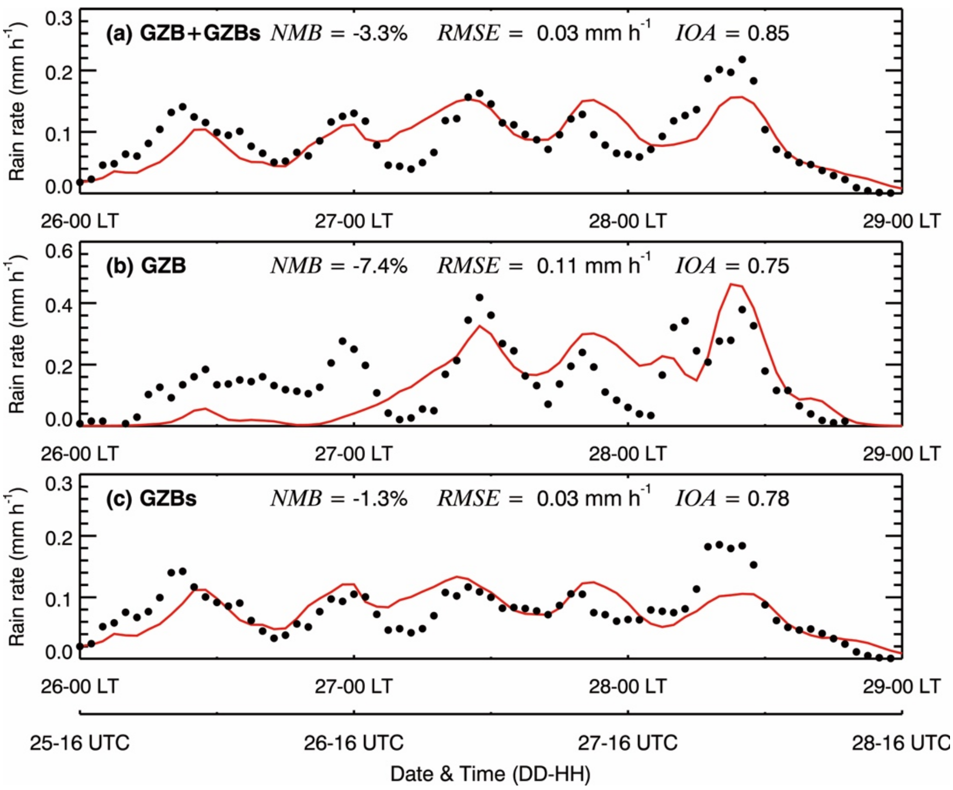

Figure 4: Comparison of observed (black dots) and simulated (solid red lines) diurnal profile of hourly rain rate averaged at monitoring sites in (a) GZB+GZBs, (b) GZB, and (c) GZBs from 26 to 28 January 2022.

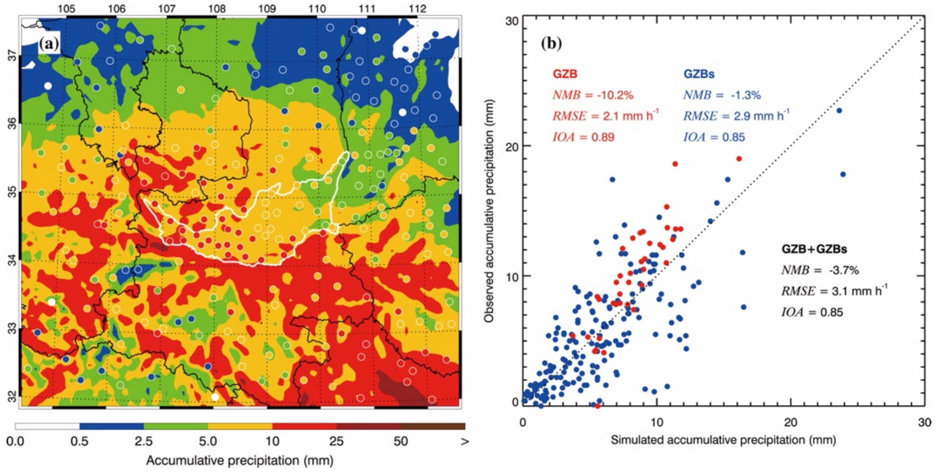

Figure 5: (a) Pattern comparisons of simulated (color counters) vs. observed (colored dots) accumulative precipitation, and (b) scatter plot of simulated and observed accumulative precipitation in GZB, GZBs, and GZB+GZBs from 26 to 28 January 2022. The white contour outlines the GZB, and the area outside of GZB in (a) is referred to as GZBs.

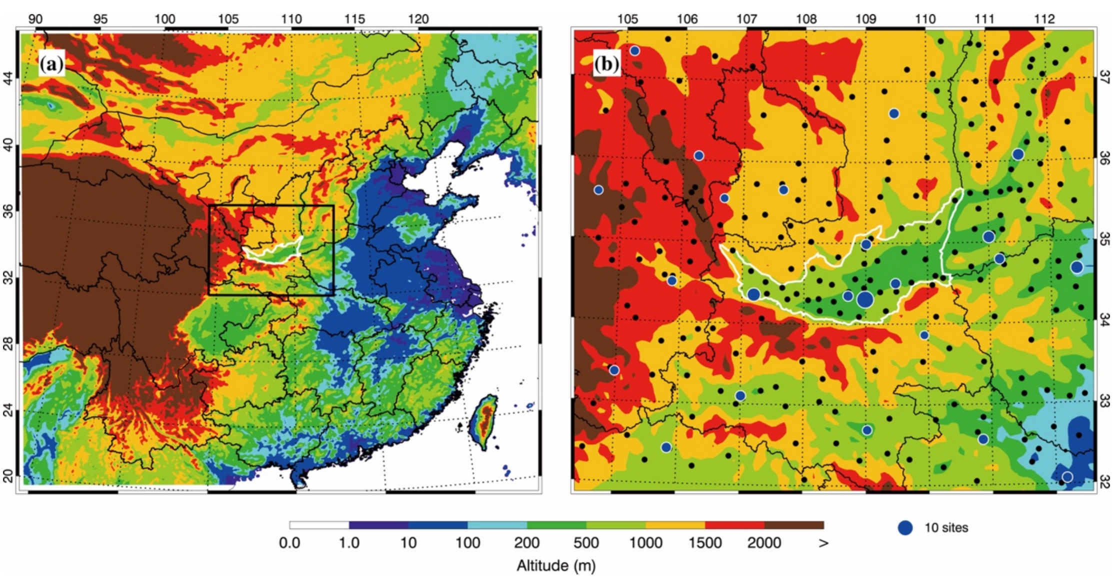

Figure 1: (a) WRF-Chem simulation domain with topography and (b) Guanzhong basin (GZB) and its surrounding areas (GZBs). In (b), the black dots denote the meteorological sites with rain gauge and the blue dots denote centers of cities with air pollutants observations and the size of blue circles denotes the number of ambient monitoring sites of cities. The white contour outlines the GZB and the area outside of GZB in (b) is referred to as GZBs.

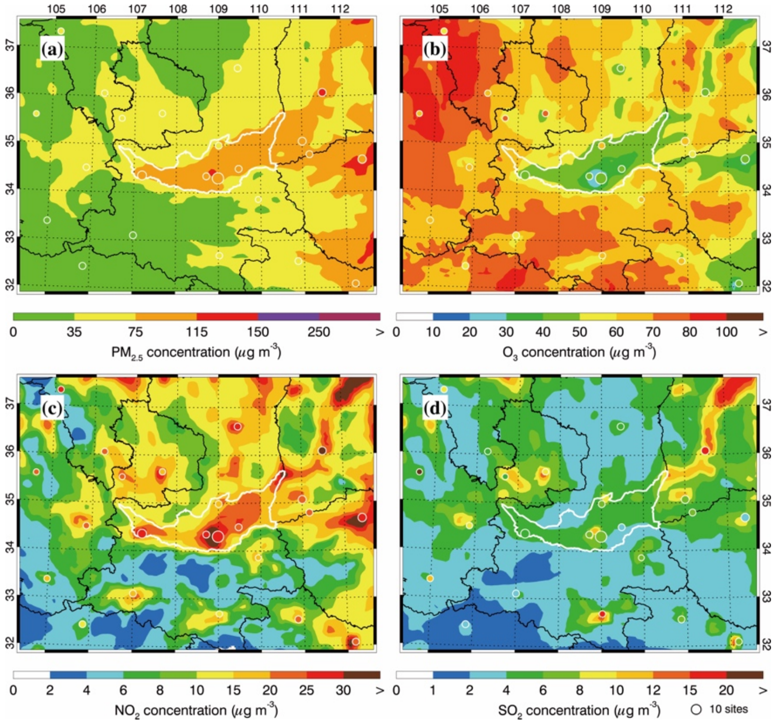

Figure 2: Pattern comparisons of simulated (color counters) vs. observed (colored dots) average near-surface mass concentrations of (a) $PM_{2.5}$, (b) O_3, (c) NO_2 and (d) SO_2 from 26 to 28 January 2022. The white contour outlines the GZB and the area outside of GZB in panels is referred to as GZBs.

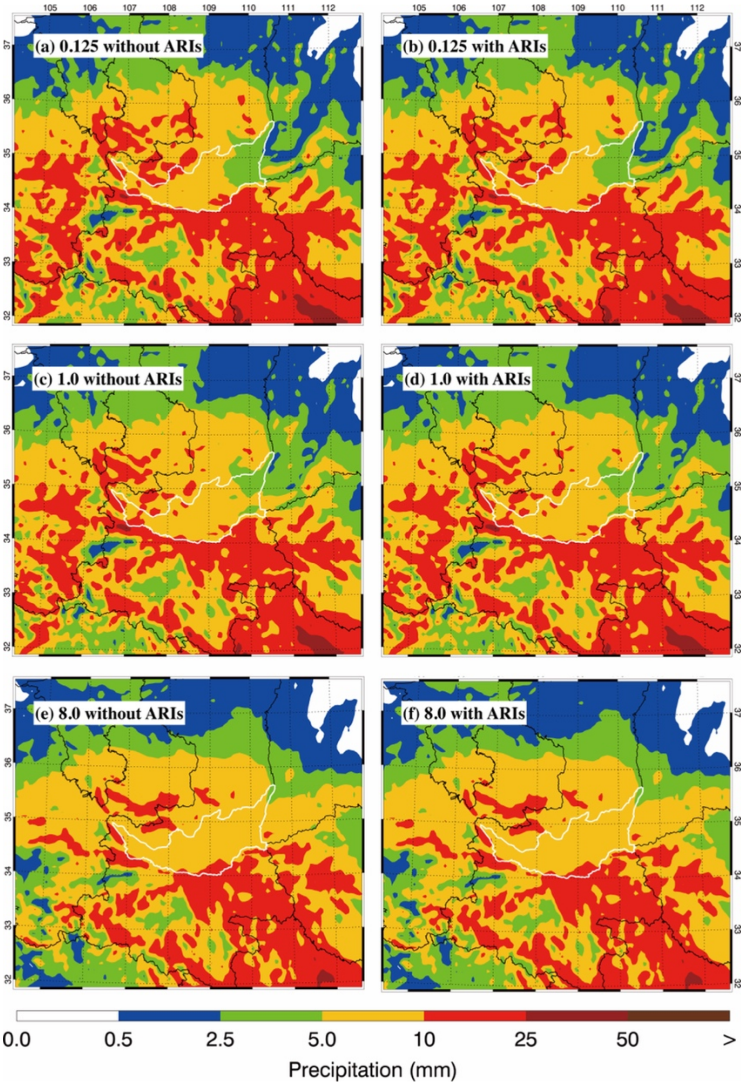

Figure 14: Distribution of accumulative precipitation from 26 to 28 January 2022 for various scale factor of anthropogenic emissions when ARIs are (a), (c), and (e) excluded and (b), (d), and (f) included. The white contour outlines the GZB. The white contour outlines the GZB and the area outside of GZB in panels is referred to as GZBs.

4 Comment: The distinction between $PM_{2.5}$ (in Section 3.2) and near-surface $PM_{2.5}$ (in Section 3.3) is unclear. The authors should explicitly state how near-surface $PM_{2.5}$ concentrations are calculated from the model simulation results.

Response: We thank the reviewer for this comment. We apologize for the unclear terminology in the original manuscript. In both Sections 3.2 and 3.3, "[$PM_{2.5}$]" refers to the near-surface $PM_{2.5}$ concentration derived from the lowest model layer. To avoid confusion, we have clarified this definition where "[$PM_{2.5}$]" is first introduced in the manuscript (Line 166), which now reads:

"*Meanwhile, despite the occurrence of the snowfall event, the observed near-surface $PM_{2.5}$ concentrations ([$PM_{2.5}$]) are still high during the three days……*"

For consistency, "[$PM_{2.5}$]" is used throughout the remainder of the manuscript to represent near-surface $PM_{2.5}$ concentrations, and redundant repetitions of "near-surface" have been removed.

5 Comment: As shown in lines 190–193 and Figure 6, the statement "the single scattering albedo is about 0.88, indicating a strong absorbing atmosphere over GZB+GZBs" requires more careful validation: First, when comparing absorbing AOD with total AOD, the absorbing component contributes only about 10%, suggesting that non-absorbing aerosols may dominate. Second, as mentioned above, aerosols can decrease PBLH through ACIs, while absorbing aerosols can heat the near-surface atmosphere by absorbing solar radiation, potentially leading to an increase in PBLH. More detailed analysis should therefore be provided, including aerosol layer height, temperature profiles, and related diagnostics.

Response: We thank the reviewer for this careful and insightful comment.

For the aerosol absorption, we have revised the sentence in lines 247-249 to: "*The average AOD and AAOD at 550nm in GZB+GZBs are 0.58 and 0.071 in the CNTL case, respectively, and the single scattering albedo at 550nm is about 0.88, indicating a moderately absorbing component within an otherwise scattering-dominated aerosol population over GZB+GZBs.*"

Regarding the relationship between absorbing aerosols and PBL development, we have revised the manuscript and added the following discussion in lines 262-266 and lines 268-286 as follows,

"Consistent with these studies, the ARI-induced temperature response in the present simulation is characterized by cooling below approximately 1.8 km and weak warming aloft (Figure 7a). The lower-atmospheric cooling is mainly caused by reduced surface solar radiation which decreases the surface sensible heat, whereas the elevated warming is associated with aerosol absorption. The resulting thermal contrast enhances lower-tropospheric stability and suppresses turbulent mixing. Consequently, the average PBLH over GZB+GZBs decreases from about 450 m to 300 m with the AESF increasing from 0.125 to 8.0 in the F_BASE, but the warming layer is generally above 1.8 km and can extend to 7~8 km with the AESF exceeding 0.5. It is worth noting that the vertical distribution of aerosol-induced heating does not necessarily coincide with the vertical distribution of absorbing aerosols. As discussed by Wu et al. (2025), radiative heating depends not only on aerosol loading but also on the vertical structure of radiative fluxes, aerosol optical properties, and air density, particularly as well as the decreased surface sensible heat. Therefore, the weak warming above approximately 1.8 km shown in Figure 7a should be interpreted as the integrated response of

aerosol–radiation interactions rather than a direct reflection of aerosol concentration at a given altitude."

6 Comment: Absorbing aerosols typically induce significant heating at the layer where they are present, leading to cooling of the atmosphere below, while exerting relatively minor influence above. However, as shown in Figure 7, no distinct warming layer is observed. In addition, although the positive and negative variations in temperature and water vapor content appear relatively consistent, the patterns of vertical velocity differ. For instance, in some regions both cooling and warming are evident, yet the corresponding vertical velocities remain positive. This discrepancy requires further clarification.

Response: We thank the reviewer for the careful examination of Figure 7. Regarding the indistinct warming layer and the apparent inconsistency between the temperature, water-vapor, and vertical-velocity responses, we have added discussions in lines 268-286 and lines 290-302 as follows,

"*It is worth noting that the vertical distribution of aerosol-induced heating does not necessarily coincide with the vertical distribution of absorbing aerosols. As discussed by Wu et al. (2025), radiative heating depends not only on aerosol loading but also on the vertical structure of radiative fluxes, aerosol optical properties, and air density, particularly as well as the decreased surface latent heat. Therefore, the weak warming above approximately 1.8 km shown in Figure 7a should be interpreted as the integrated response of aerosol–radiation interactions rather than a direct reflection of aerosol concentration at a given altitude. During the study period, the profile of vertical velocity shows occurrence of downdraft within the PBL and updraft above the PBL (Figure S3a). The cooling effect of ARIs within the near-surface atmosphere induces a downward motion and meanwhile an upward motion is generated above the PBL, which is resulted from the warming effect caused by absorbing aerosols and enhanced convergence by the ARI-induced downward motion (Figure 7b). The vertical velocity response shown in Figure 7b does not directly mirror the temperature anomalies at each height. Instead, it reflects a dynamical adjustment to the vertically contrasting radiative forcing. Aerosol scattering cools the lower atmosphere through surface dimming, while aerosol absorption produces weak warming above approximately 1.8 km. The resulting thermal contrast favors ascent above the PBL, while downward motion develops within the boundary layer due to the combined effects of enhanced lower-tropospheric stability and compensating subsidence associated with the ascent aloft. Consequently, ARIs strengthen downward motion in the lower atmosphere and upward motion aloft. These ARI-induced variations in divergence and water* *vapor flux are shown in Figure S5. ARIs induce divergence (positive values) below approximately 700 m and convergence (negative values) above this level, with the convergence strengthening as AESF increases. Correspondingly, negative water vapor flux anomalies occur within the divergent layer, indicating moisture export from the lower troposphere, while positive anomalies occur within the convergent layer aloft, indicating moisture accumulation. This circulation pattern contributes to the drying of the PBL. Therefore, the upward motion above the PBL is enhanced by ARIs and more warm and moist air in the lower layer is being transported upward. The ARI-enhanced downward motion within the near-surface atmosphere is subject to transporting more air in the upper layer downward, causing a dry and cold effect, as shown in Figure 7c.*"

7 Comment: The manuscript presents an interesting case study on aerosol impacts on snowfall using WRF-Chem, but the physical interpretation of aerosol–radiation interactions (ARIs) remains insufficiently supported. In particular, the study lacks a quantitative analysis of radiative heating rates or flux divergence, making it difficult to attribute the simulated temperature changes solely to ARIs rather than dynamical adjustments.

Response: We thank the reviewer for this important comment. We agree that Figure 7 does not isolate the instantaneous radiative heating rate or radiative flux divergence. Instead, the temperature differences shown in Figure 7a represent the total atmospheric response induced by ARIs. We have now clarified it in Lines 255-258 as follows:

"*Figure 7a shows the effect of ARIs on the temperature profile averaged in GZB+GZBs during the study period by differentiating the F_BASE and F_ARI0 under various aerosol conditions. It should be noted that the temperature anomalies shown in Figure 7a represent the total atmospheric response to ARIs, including both the direct aerosol radiative forcing and the subsequent dynamical adjustments, such as changes in vertical motion, heat transport, and boundary-layer mixing. ARIs decrease the air temperature of the low-level atmosphere, and the air temperature decrease is mainly concentrated below 1.8 km and becomes increasingly significant with decreasing height or increasing AESF (Figure 7a).*"

We have added a quantitative analysis of flux divergence and related discussions in lines 297-302 of the revised manuscript as follows,

"*These ARI-induced variations in divergence and water vapor flux are shown in Figure S5. ARIs induce divergence (positive values) below approximately 700 m and convergence (negative values) above this level, with the convergence strengthening as AESF increases. Correspondingly, negative water vapor flux anomalies occur within the divergent layer,* *indicating moisture export from the lower troposphere, while positive anomalies occur within the convergent layer aloft, indicating moisture accumulation. This circulation pattern contributes to the drying of the PBL.*"

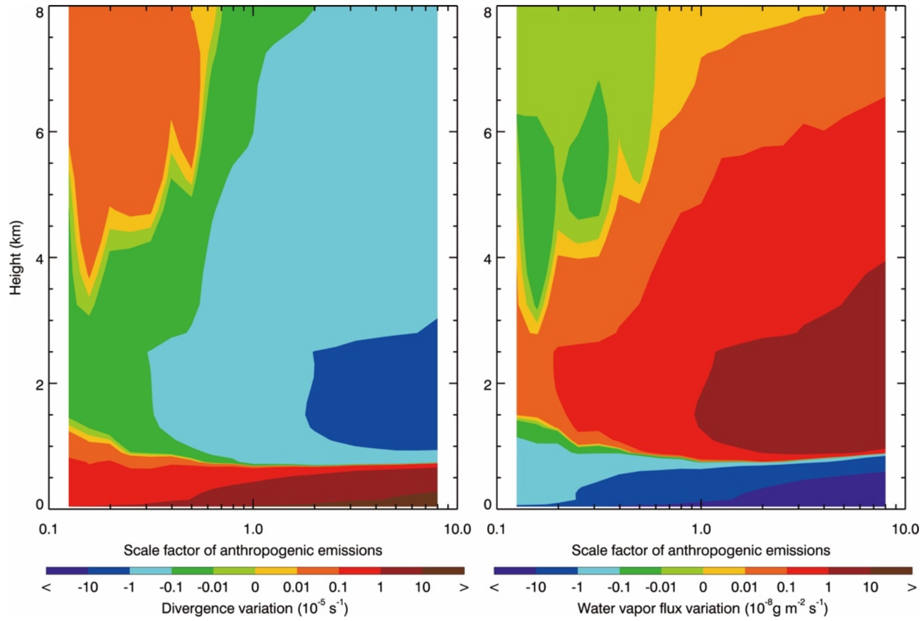

Figure S5: *Profile variation of horizontal (a) divergence and (b) water vapor flux averaged over GZB+GZBs from 26 to 28 January 2022 caused by ARIs, as a function of the scale factor of anthropogenic emissions. For the divergence variations, negative values indicate that ARIs enhance convergence, whereas positive values indicate enhanced divergence. For the water vapor flux variations, positive values indicate enhanced moisture inflow into the region, while negative values indicate enhanced moisture outflow from the study region.*

8 Comment: The separation of aerosol–radiation interactions (ARIs) and aerosol–cloud interactions (ACIs) using sensitivity experiments may introduce methodological uncertainties. Given the nonlinear coupling between radiation, thermodynamics, and microphysics, the simple differencing approach (F_BASE minus F_ARI0) may not fully isolate ARI effects. The authors should discuss the potential nonlinearity and associated uncertainties more explicitly.

Response: We have added discussions in lines 482-491 of the revised manuscript as "*The sensitivity experiment design used to separate ARIs and ACIs is subject to uncertainties arising from the nonlinear coupling between radiation, thermodynamics, and cloud microphysics. The differencing approach does not fully isolate pure ARIs but rather includes contributions from nonlinear interactions between ARIs and ACIs. While this approach is widely used in the previous studies (Bei et al., 2025; Ding et al., 2019; Wu et al., 2018), the quantitative ARIs effects reported here may contain some uncertainty, particularly in regions with strong aerosol-*

cloud-radiation feedbacks. Nevertheless, the robust regional contrast in precipitation responses that enhancement in the GZB versus suppression in the GZBs is substantially larger than the estimated uncertainty due to nonlinearities, and the qualitative conclusions of this study remain robust. Future work employing incremental aerosol perturbations or partial radiative perturbation techniques could provide a more refined separation of the ARIs effects."

9 Comment: The use of a wide range of anthropogenic emission scaling factors (AESF from 1/8 to 8) raises concerns regarding the realism of the experimental design. Such extreme perturbations may not represent realistic atmospheric conditions and could lead to artificial nonlinear responses, including the reported threshold behavior. A justification based on observed aerosol variability is needed.

Response: We have added discussions based on observed aerosol variability in lines 132-144 in the revised manuscript as follow,

"*It is worth noting the use of a wide range of AESFs might not represent realistic emission-control scenarios. In the study, the main purpose of applying a wide range of AESFs is to systematically explore the nonlinear responses of aerosol-cloud-precipitation interactions across aerosol environments ranging from relatively clean to heavily polluted conditions. Wintertime $PM_{2.5}$ concentrations in northern China exhibit substantial variability associated with haze development, boundary-layer evolution, and unfavorable meteorological conditions, often varying by more than one order of magnitude between clean and polluted periods (Li et al., 2021). In the GZB, frequent severe winter haze events have been reported under stagnant meteorological conditions and complex basin topography, with $PM_{2.5}$ concentrations commonly exceeding 200-300 μg m^{-3} during polluted episodes (Bei et al., 2017b). As shown in Figure S1, the average wintertime [$PM_{2.5}$] have decreased from about 160 μg m^{-3} in 2013 to 65 μg m^{-3} in 2026 in response to emission-control measures, highlighting the large variability of aerosol loading in this region. Therefore, the selected AESF range is designed to span the observed variability of aerosol conditions and to identify potential threshold and nonlinear behaviors of ARIs and ACIs under different pollution regimes.*"

Li, Q., Zhang, H., Cai, X., Song, Y., and Zhu, T.: The impacts of the atmospheric boundary layer on regional haze in North China, npj Clim. Atmos. Sci., 4, 9, https://doi.org/10.1038/s41612-021-00165-y, 2021.

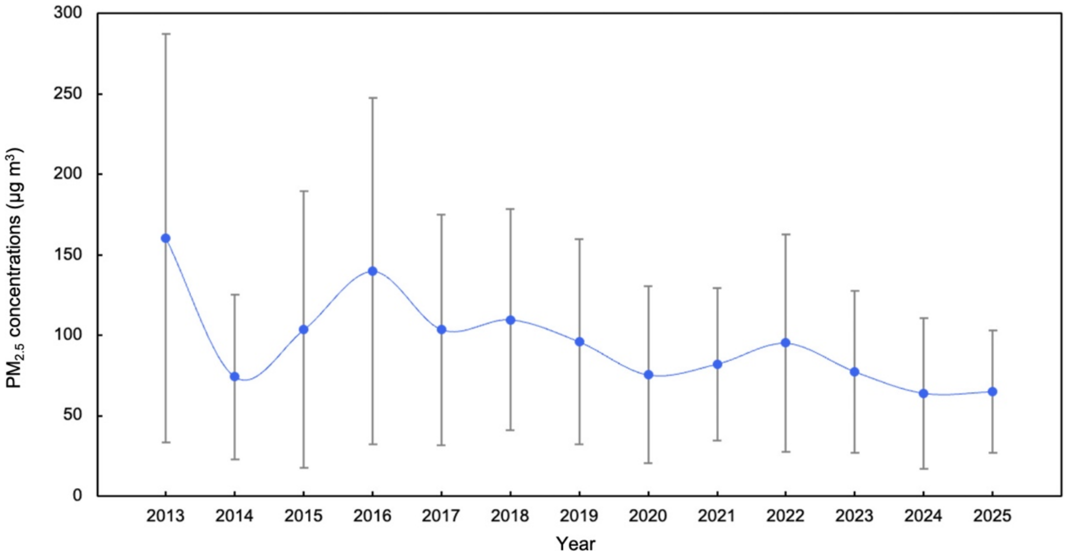

Figure S1: *Interannual variations in observed average [$PM_{2.5}$] over the GZB during the winters (December–January–February) of 2013–2025. The blue circles represent basin-averaged [$PM_{2.5}$], and the error bars indicate the standard deviation among monitoring sites.*